

A Novel Patch Array Antenna with Wideband and Dual Sense Circular Polarization Characteristics for WiMAX & WLAN Applications

Yaqiang Zheng^{1, 3, 4}, Min Gao^{2, 3, 4, *}, and Xiaohu Zhao^{3, 4}

Abstract—A wideband patch array antenna with dual sense circular polarization (CP) is investigated in this paper. Four rotated hexagonal patches are sequentially distributed on the upper surface of substrate 1 to form a patch array. In order to widen impedance bandwidth, an annular feeding network with four rectangular branches is designed. At the bottom of the antenna, two orthogonally placed microstrip baluns are introduced to obtain the characteristics of left-hand circular polarization (LHCP) and right-hand circular polarization (RHCP). Meanwhile, four coaxial probes, passing through substrate 2 and substrate 3, are used to transmit the feeding signal between microstrip balun and the annual feeding network. The proposed patch array antenna is fabricated for verifying the feature of wideband and dual circular polarizations. The measured results show that the antenna has an impedance bandwidths of 70.2% (1.72–3.58 GHz) with an axial ratio (AR) bandwidth of 61% (1.85–3.48 GHz) and over 6.2 dBi gain at two ports. Moreover, the measured port isolation remains below -15 dB over the entire impedance bandwidth, and the measured radiation patterns with excellent directionality and symmetry at two ports indicate that the proposed antenna can be used for wireless applications.

1. INTRODUCTION

In recent years, patch antennas have been widely used in wireless communications due to the advantages of low profile, light weight, and low cost. With the continuous innovation of wireless communication technology, the communication market is gradually leading the development of patch antennas towards the direction of integration, dual polarizations, and broadband. A patch antenna with the feature of dual-CPs can be utilized to reduce fading loss and obtain frequency reuse. However, the narrowband characteristic of microstrip patch antenna is not suitable for wideband wireless communication applications.

CP wave can be obtained by orthogonalizing two linearly polarized waves with equal amplitude and 90° phase difference. In [1], a circularly polarized square slot antenna is researched, and two inverted-L grounded strips are loaded in the two opposite corners of the square slot to achieve the feature of CP. The measured results show that the axial ratio bandwidth (ARBW) of the antenna is larger than 25%. A truncated driven patch and five parasitic patches are respectively etched on different layers to improve the axial ratio bandwidth in [2]. Then, better impedance matching is acquired with the measured 3-dB ARBW of 20.7% and over 7.9 dBi gain, which can be attributed to the structure of stacked patch. The 90° phase delay line capable of outputting signals with equal amplitude and 90° phase difference is also utilized to design the CP antennas in [3–5]. A wideband patch antenna with the feature of circular

Received 17 November 2019, Accepted 7 January 2020, Scheduled 30 January 2020

* Corresponding author: Min Gao (gm@htc.edu.cn).

¹ Department of Mechanical and Electrical Engineering, Huainan Union University, Huainan 232000, China. ² School of Mechanical and Electrical Engineering, Hefei Technology College, Hefei 230601, China. ³ School of Information and Control Engineering, China University of Mining and Technology, Xuzhou 221000, China. ⁴ The National Joint Engineering Laboratory of Internet Applied Technology of Mines, Xuzhou 221000, China.

polarization and compact size is proposed in [3]. A loop feeding structure, consisting of a 90° phase delay line, is combined with four parasitic patches to broaden the impedance bandwidth and ARBW. Both antennas in [4, 5] combine parasitic loop resonators and metasurface on the basis of 90° phase delay line respectively to obtain the AR bandwidth which is more than 28.6%.

The antennas in [1–5] all have the attractive characteristics of wideband and single circular polarization. However, the application of a single-polarized antenna is limited in the wireless communication environment. At the same time, the dual sense circular polarization is also researched to improve the anti-interference ability of CP antenna. In [6], the multimode transmission line is introduced to exploit the even and odd modes in two separate ports, then two orthogonal CP modes emerge at 2.575 GHz. In [7], planar multilayer circuit board technology is employed to construct a multilayer dual CP antenna with high isolation and high efficiency. A quarter mode substrate integrated waveguide (SIW) cavity is investigated in [8] to drive the CP radiation only if the TE_{220} mode [9] is stimulated. Moreover, two open-stubs and defected ground structure are also utilized to obtain 3-dB ARBW of 11.2% and high isolation.

In this paper, a dual sense circularly polarized patch array antenna with widened ARBW and impedance bandwidth is designed. Two wideband 90° phase shifters are loaded on the bottom of the antenna to provide signals with phase difference stability at $90^\circ \pm 5^\circ$. Furthermore, an annular feeding network with four rectangle branches, printed on the middle layer, is weakly coupled with the sequential rotated hexagonal patch array. Increased port isolation is acquired by placing two microstrip baluns orthogonally, and the measured results show that the antenna with impedance bandwidth of 70.2%, ARBW of 61%, dual sense circularly polarized radiation, and over 6.2 dBi in two ports can be applied to WiMAX and WLAN.

2. ANTENNA DESIGN AND FEED TECHNIQUE

According to the previous literature, fan-shaped strips with angle of 270° can also be utilized to obtain 90° phase difference. Due to the unreconfigurability of fan-shaped strips, only one of the $\pm 90^\circ$ phase differences can be acquired. Therefore, the circular polarization characteristics in [3–5] all exhibit a single polarization. In this paper, a feeding network, consisting of two 90° broadband baluns, is designed to replace fan-shaped strips. Furthermore, the difference between the feeding network and feed-line in [6] is that a larger bandwidth with more stable phase difference can be realized in this paper. The feed-line in [6] exploits the even and odd modes of a coplanar waveguide transmission line, and a narrow axial ratio bandwidth is achieved. For the antennas in [7–10], metallized vias are introduced as a key component for shorting vias and SIW. It cannot be ignored that large-area metallized vias are not conducive to the integration of antennas. On the other hand, the antenna proposed in this paper is fixed with nylon screws, and the feeding network is integrated with the radiating module of the antenna, which greatly improves the integration of the patch array antenna. Based on the aforementioned analysis, the design procedure of the proposed antenna can be summarized as the following steps.

2.1. Patch Array Design

The geometry of the proposed patch array antenna with optimized parameters is shown in Fig. 1 and Table 1. It can be seen from Fig. 1(a) that the uppermost layer of the proposed antenna is substrate 1 with thickness of 5 mm and dielectric constant of 2.65. Four hexagonal patches are rotationally distributed on the upper surface of substrate 1 to construct the patch array. Substrate 2, with the same electrical parameters and dimensions as substrate 1, is located in the middle layer of the antenna. An annular feeding network with four rectangle branches is printed on the upper surface of substrate 2. At the same time, it is worth mentioning that an air layer with thickness of 1 mm is introduced between substrate 1 and substrate 2 to reduce the quality factor of the antenna, that is, the Q value. On the other hand, the introduction of the air layer has a positive effect on widening the impedance bandwidth from Eqs. (1) and (2), wherein f_{\max} is the cut-off frequency of high frequency, f_{\min} the cut-off frequency of low frequency, and VSWR the voltage standing wave ratio of the antenna. Two microstrip baluns are printed on the back side of substrate 3, which is located on the bottom of the antenna to obtain the characteristic of dual CPs. Meanwhile, a rectangle metal plating, as a ground plane of the proposed

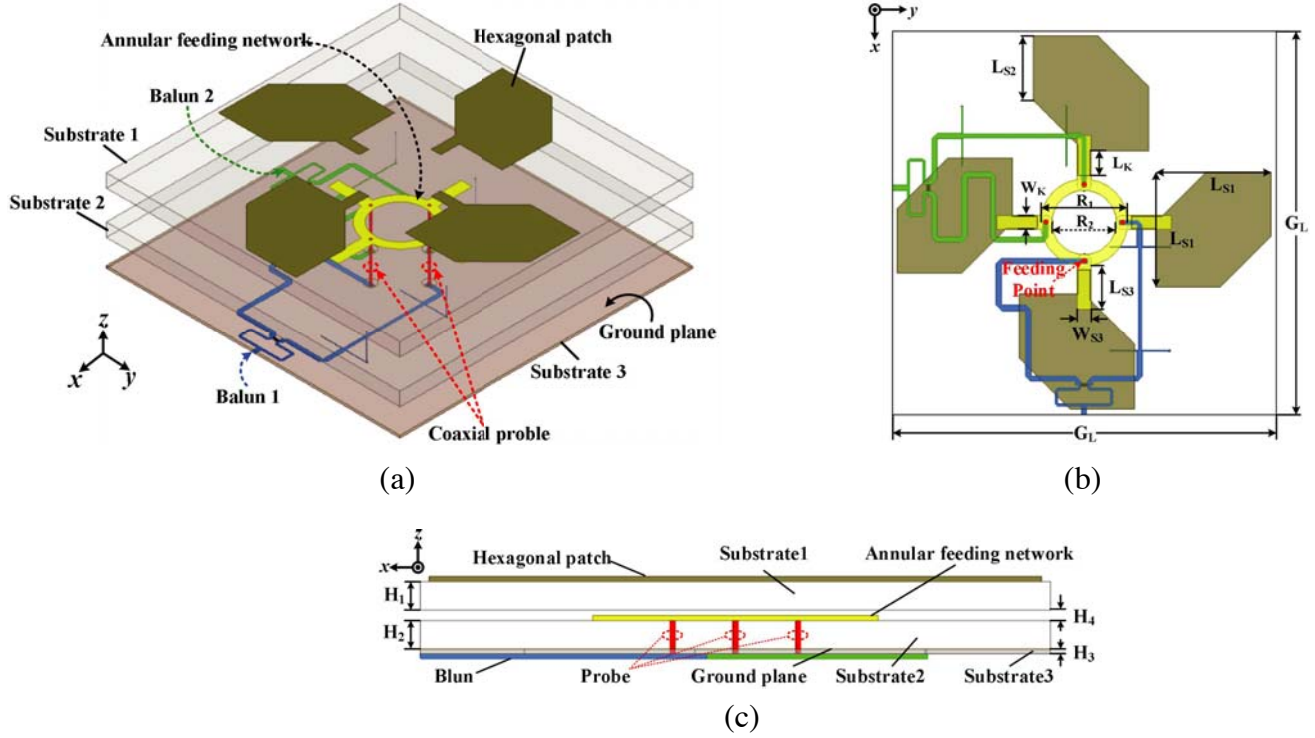


Figure 1. Geometry of the dual-CP patch array antenna. (a) 3-D view; (b) top view; (c) side view.

Table 1. Dimensions of the designed antenna.

Parameters	G_L	d	L_{S1}	L_{S2}	L_{S3}	W_{S3}	L_K
Values/mm	110	22	33	18.5	12.7	4	7
Parameters	W_K	H_1	H_2	H_3	H_4	R_1	R_2
Values/mm	3.5	5	5	0.8	1	25	18.5

antenna, is printed on the upper surface of substrate 3. In order to ensure that the two microstrip baluns can be directly connected to the annular feeding network, four cylindrical coaxial probes are embedded in substrate 2 and substrate 3.

$$Q = \frac{1}{bw} = \frac{f_{\max} - f_{\min}}{\sqrt{f_{\max} \times f_{\min}}} \tag{1}$$

$$bw = \frac{\sqrt{VSWR}}{Q \times (VSWR - 1)} \times 100\% \tag{2}$$

2.2. 90° Broadband Balun Design

The circuit schematic of the designed balun is shown in Fig. 2, and it can be seen from Fig. 2 that the balun consists of a two-way equal power division Wilkinson power divider cascaded with a non-coupled-line wideband 90° phase shifter. Initially, the original signal is fed into the antenna through input port 1, then two signals with equal amplitude and the same phase are obtained when the original signal is split by a Wilkinson power divider. After the isolation resistor R , the separated signal flows through the broadband 90° phase shifter to obtain two signals with equal amplitude and phase difference of 90°. Finally, the converted signals are sent to the annular feeding network through output port 2 and output port 3, respectively.

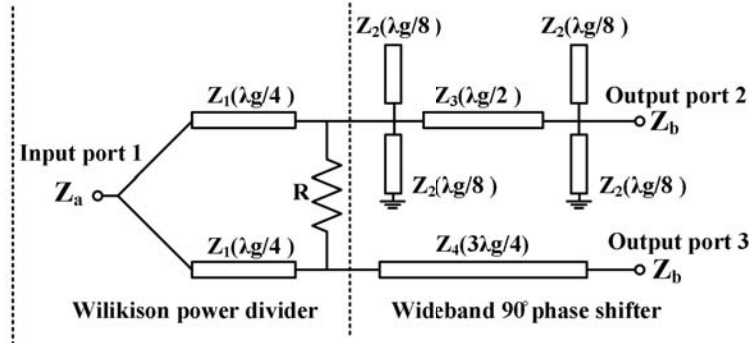


Figure 2. Circuit schematic of the microstrip balun.

For the convenience of analysis, the design formulas are exemplified as shown in Eqs. (3)–(7), where Z_a and Z_b respectively represent the characteristic impedances of the balun input and output port. Z_1 represents the characteristic impedance of the quarter-wavelength microstrip line in the Wilkinson power splitter, and a $50\text{-}\Omega$ chip resistor is introduced to improve the port isolation. Z_3 represents the characteristic impedance of the main microstrip line in the 90° phase shifter. Two shunted-open branches and two short-circuit branches, with the same characteristic impedance of Z_2 , are located at both ends of the main microstrip line, respectively. Z_4 stands for the characteristic impedance of the reference line with a length of three-quarter wavelength, and it is worth noting that Z_a and Z_b are usually set to $50\text{ }\Omega$ to meet the matching conditions.

$$Z_1 = \sqrt{2Z_a \cdot Z_b} \quad (3)$$

$$R = 2 \cdot Z_a \quad (4)$$

$$Z_2 = 2.51 \cdot Z_a \quad (5)$$

$$Z_3 = 1.24 \cdot Z_a \quad (6)$$

$$Z_4 = Z_a \quad (7)$$

An FR4 board with thickness 0.8 mm and dielectric constant 4.4 is employed as substrate 3. Two broadband baluns are printed on the back side of substrate 3, and a photograph of the proposed balun is also given in Fig. 3. It can be concluded from Fig. 3 that feeding points A and B are output ports of the blue balun, excited by port 1 to obtain the characteristic of LHCP. Similarly, feeding points C and D

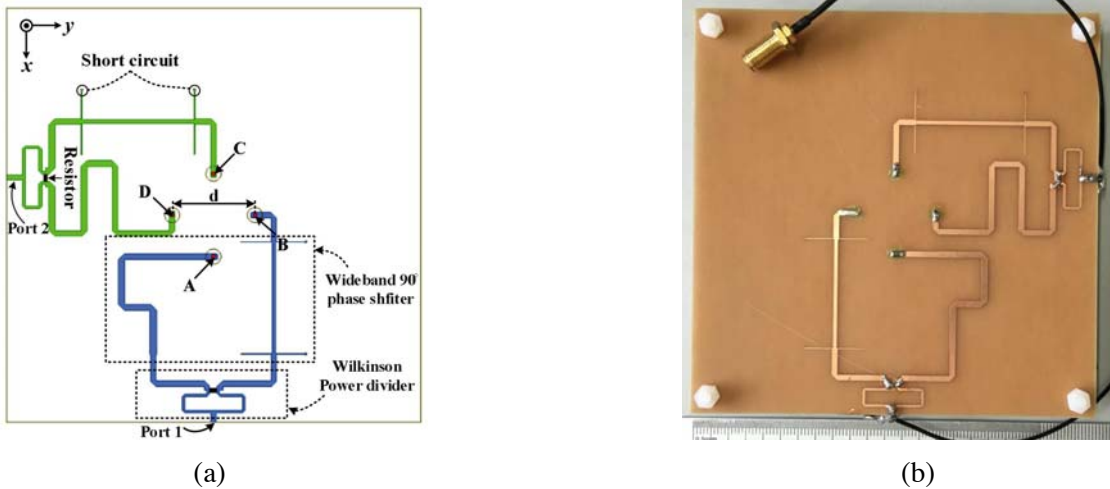


Figure 3. Configuration of broadband balun. (a) Layout graph of the balun; (b) photograph of the fabricated balun.

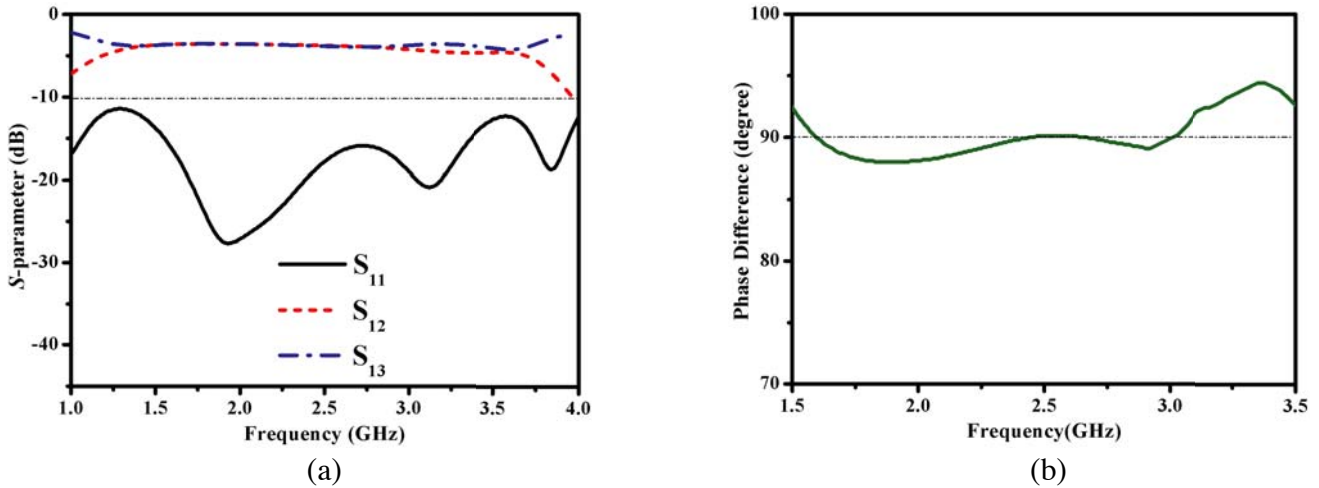


Figure 4. Simulated results of the designed broadband balun. (a) S -parameter; (b) phase difference of the two output ports.

act as output ports for the green balun, excited by port 2 to achieve the feature of RHCP. Since the two baluns have the same configuration and electrical parameters, only the simulated result of blue balun is given in Fig. 4 for brevity. As shown in Fig. 4, the return loss of the designed balun remains below -10 dB from 1.5 GHz to 3.5 GHz, and the simulated results of S_{21} and S_{31} are around 3 dB. Moreover, the balun can continuously output signals with the same amplitude and phase difference of $90^\circ \pm 5^\circ$ within 1.5–3.5 GHz, as shown in Fig. 4(b).

3. SIMULATED AND MEASURED VALIDATION

Since the antenna proposed in this paper has the attractive characteristics of broadband and dual sense circular polarization, an antenna prototype as shown in Fig. 5 is fabricated. Meanwhile, an Agilent N5230A network analyzer and a Satimo Starlab near-field measurement system are utilized to test the performance of the antenna.

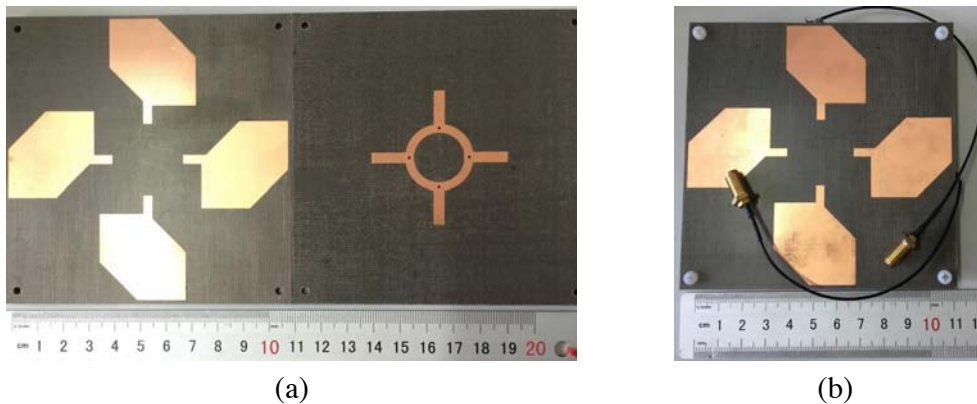


Figure 5. Prototype of the fabricated antenna. (a) Substrate 1 and substrate 2; (b) assembled antenna.

The measured S -parameters of the proposed patch array antenna are given in Fig. 6. Similarly, the simulated results are also given in Fig. 6 for comparison with measured ones. It can be observed from Fig. 6 that the measured results are basically consistent with the simulated ones. When port 1 is energized, port 2 is loaded with a $50\ \Omega$ termination load. At the same time, the measured results

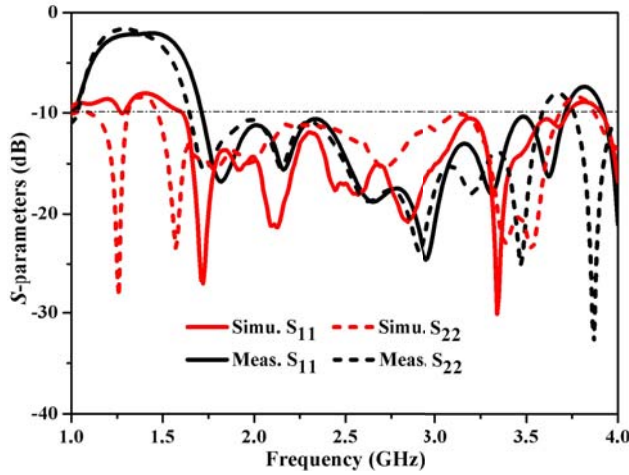


Figure 6. Simulated and measured S -parameters of the proposed antenna.

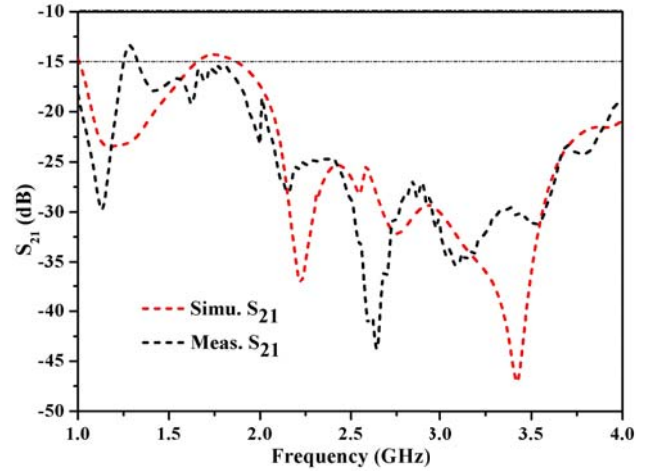


Figure 7. Simulated and measured isolation between port 1 and port 2.

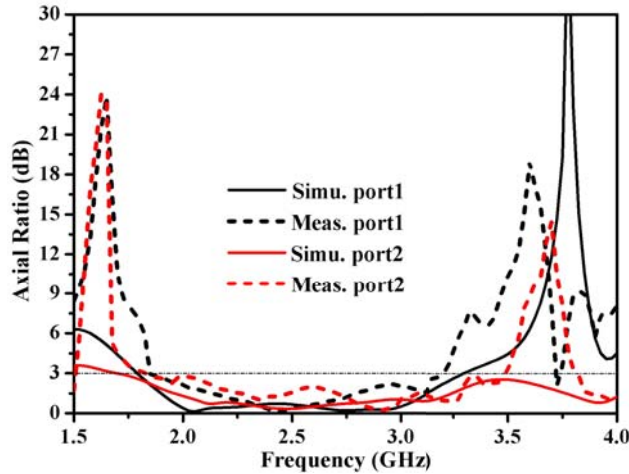


Figure 8. Simulated and measured AR of the proposed antenna for port 1 and port 2.

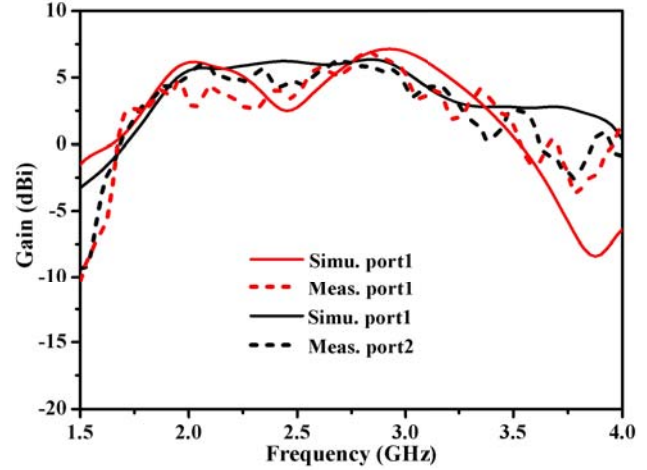


Figure 9. Simulated and measured gain of the proposed antenna in two ports.

show that the return loss in 1.72–3.71 GHz is less than -10 dB. Conversely, while port 2 is excited, port 1 is loaded with a $50\ \Omega$ termination load, and the corresponding measured results show that the return loss of the antenna is less than -10 dB in 1.65–3.58 GHz. After comprehensive comparison, the proposed antenna has an impedance bandwidth of 70.2% (1.72–3.58 GHz) in two ports. The isolation between port 1 and port 2 is also measured, and the result is shown in Fig. 7. It can be concluded from Fig. 7 that the port isolation of the proposed antenna remains above 15 dB over the entire impedance bandwidth from 1.65 GHz to 3.71 GHz. Moreover, it is well known that with higher isolation, the mutual interference between two ports is smaller, and the antenna with the characteristic of dual polarizations can acquire polarization diversity more efficiently.

Figure 8 presents the curve between the axial ratio and frequency. Comparing the measured results with the simulated ones, it is found that the measured ARBW of two ports are smaller than the simulated results. The antenna operates with a left-hand circular polarization mode, as port 1 is excited, and the measured antenna axial ratio is less than 3 dB in 1.80–3.27 GHz. The case of port 2 is also shown in Fig. 8. The antenna works in right-hand circular polarization mode, and the measured 3 dB axial ratio bandwidth of port 2 is 61% (1.85–3.48 GHz). However, as shown in Fig. 8, the simulated axial ratio of port 2 is less than 3 dB in 1.76–4.0 GHz, which is larger than the measured

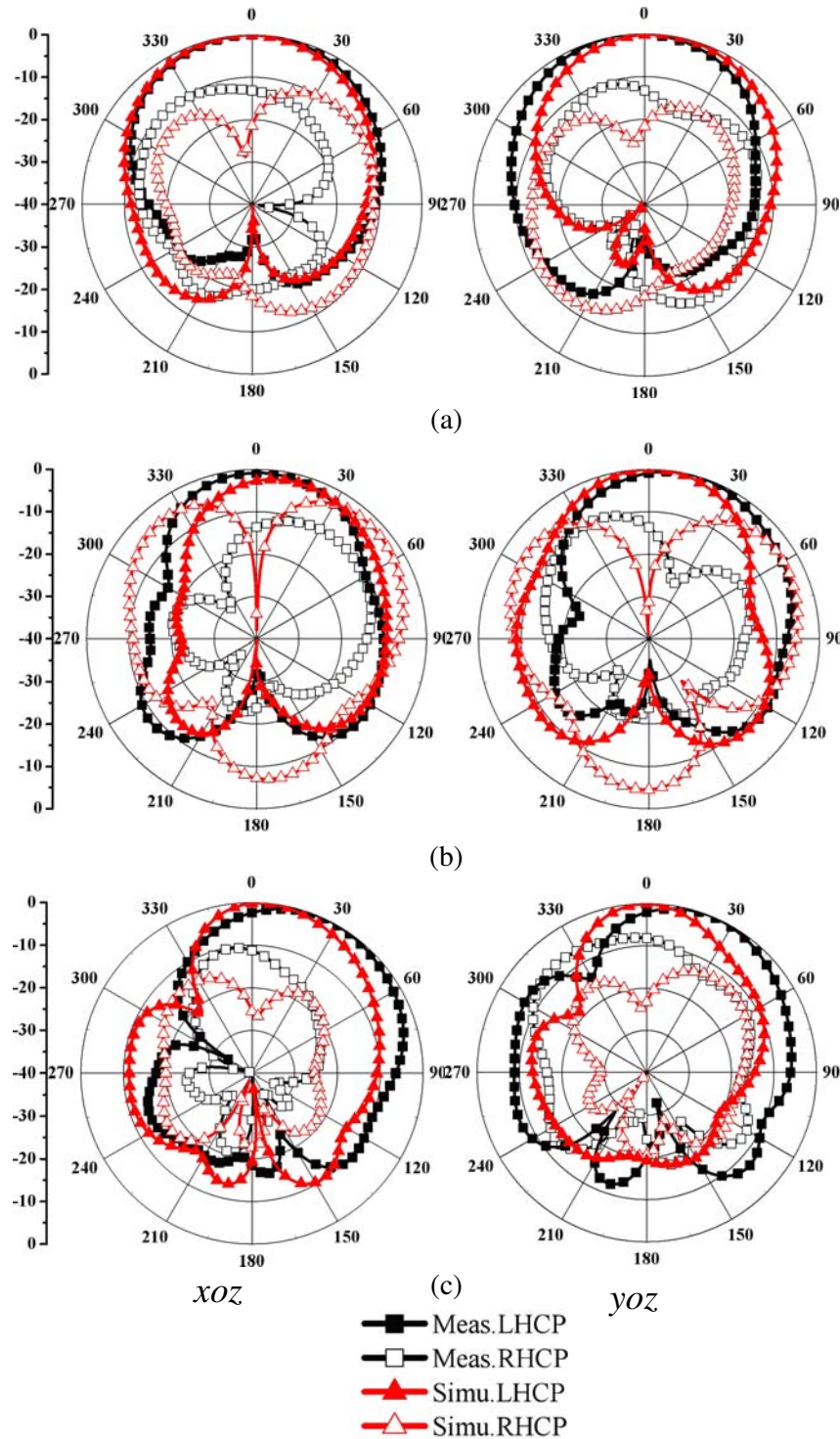


Figure 10. Simulated and measured radiation patterns of the proposed antenna in xoz and yoz planes. (a) 1.9 GHz; (b) 2.6 GHz and (c) 3.3 GHz for port 1.

result of port 2. The main reason for this phenomenon is the error during processing and measurement. After comparative analysis, the characteristics of dual CPs and $S_{11}/S_{22} \leq -10$ dB are obtained in 1.85–3.48 GHz, completely covering the bandwidth of antennas in WLAN (2.4–2.484 GHz) and WiMAX (2.5–2.69 GHz) applications.

The gain characteristic of the proposed antenna is illustrated in Fig. 9, and the maximum measured gains of port 1 and port 2 are 6.93 and 6.19 dBi, respectively. Compared with the corresponding simulated gains 7.14 and 6.35 dBi, the antenna gain is reduced by 0.3 dBi approximately. The reduction of the antenna gain is mainly due to the high dielectric loss of FR4 and the chip resistor of microstrip balun.

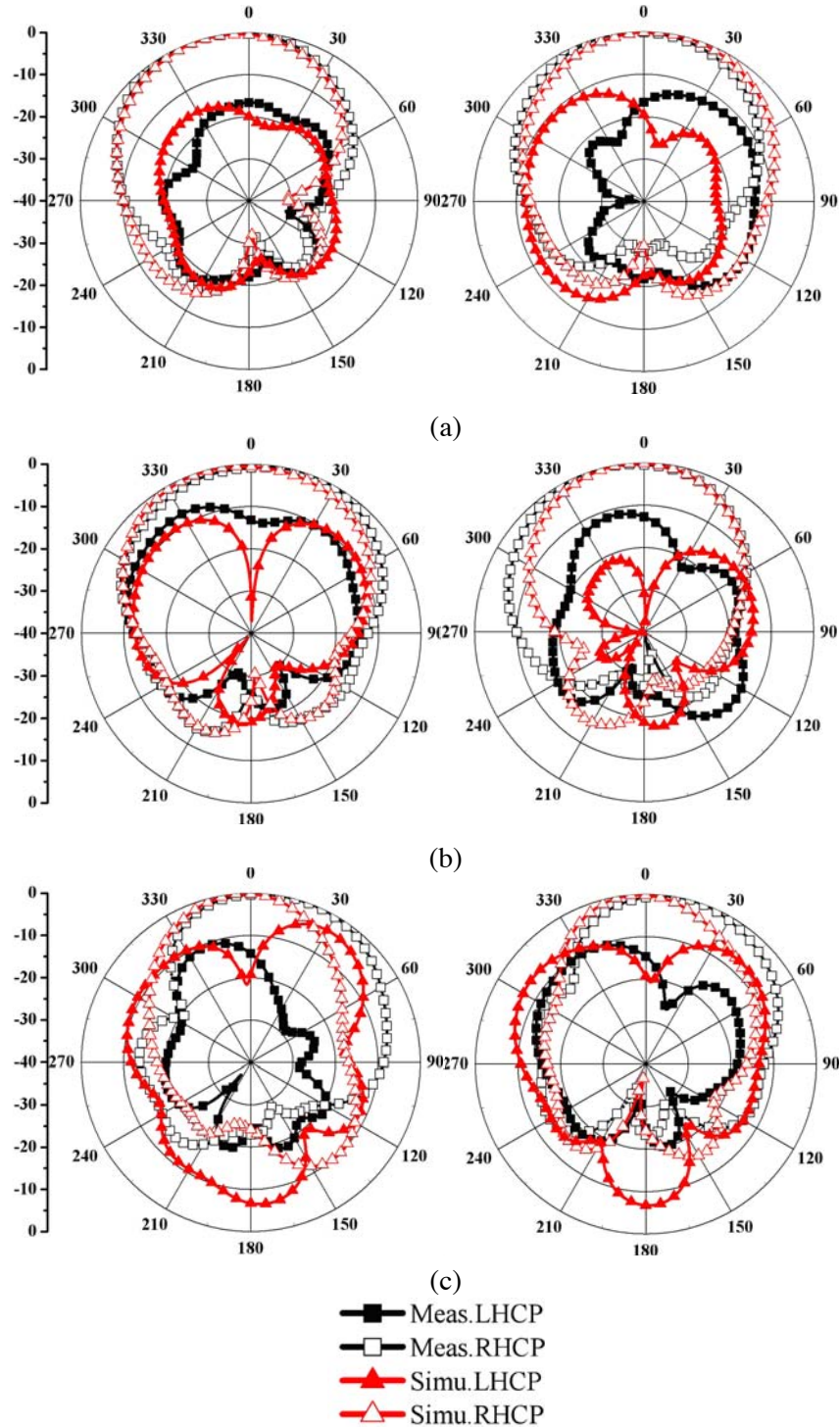


Figure 11. Simulated and measured radiation patterns of the proposed antenna in xoz and $yo z$ planes. (a) 1.9 GHz; (b) 2.6 GHz and (c) 3.3 GHz for port 2.

In order to vividly illustrate the dual CP characteristic of the proposed antenna, the measured radiation patterns are also shown in Fig. 10 and Fig. 11 when port 1 and port 2 are excited respectively. As shown in Fig. 10 and Fig. 11, the xoz -plane and $yo z$ -plane patterns at 1.9 GHz, 2.6 GHz, and 3.3 GHz are exemplified. By comparing the results in Fig. 10, it can be concluded that the co-polarizations show left-hand circular polarization with better directivity and front-to-back ratio. Similarly, as shown in Fig. 11, the measured co-polarization of the proposed antenna shows right-hand circular polarization, and the high front-to-back ratio is also acquired. Combining the radiation patterns in Fig. 10 and Fig. 11, it is verified that the designed antenna can operate well with the dual sense circular polarization characteristic over the entire ARBW.

4. COMPARISON

Some of the previously reported antennas are summarized in Table 2 for comparison with the proposed work. In [3–5], the circular polarization characteristics all exhibit a single polarization, which greatly limits the application scenarios of the designed antenna. Furthermore, the antenna profile height in [4] is as high as 27 mm, which makes the antenna volume too large for integration. A dual sense circularly polarized antenna is presented in [6] with ARBW of 1.3%. Because the ARBW is too narrow, the antenna is not suitable for broadband communication. Meanwhile, SIW technology is also employed to design a broadband dual circularly polarized antenna in [8]. However, the measured isolation between the two ports is only 12.5 dB lower than the antenna designed in this paper. In [10], an SIW horn antenna with the characteristics of wideband and dual sense circular polarization is investigated. The measured results of impedance bandwidth and 3 dB axial ratio bandwidth are 25.6% and 11.8%, respectively, which are lower than the corresponding results in this paper. Therefore, the proposed antenna stands out because of the low profile, dual CPs, large impedance bandwidth, and widened axial ratio bandwidth, and it could be applied to broadband wireless communication.

Table 2. Comparison between reported and the proposed dual CP.

Ref	IB (%)	ARBW (%)	Isolation (dB)	MG (dBi)	PS	Type
[3]	19.5	12.9	-	9.8	RHCP	Planar
[4]	38.2	28.6	-	8.3	RHCP	No-Planar
[5]	58.1	41.7	-	12.1	LHCP	Stacked
[6]	1.3	1.3	> 20	5.8	LHCP & RHCP	Planar
[8]	16	11.2	> 12.5	4.7	LHCP & RHCP	Planar
[10]	25.6	11.8	> 15	10.3	LHCP & RHCP	Stacked
This work	70.2	61.0	> 15	6.2	LHCP & RHCP	Stacked

IB: Impedance Bandwidth; MG: Max Gain; PS: Polarization State.

5. CONCLUSION

A wideband dual circular polarization patch array antenna covering the WiMAX and WLAN bands is presented in this paper. The designed antenna is composed of three layers of substrates superposed from top to bottom. An air layer with thickness of 1 mm is introduced to obtain weak electromagnetic coupling between the patch array and annular feeding network. Two broadband baluns are introduced on the back side of substrate 3 to output signal with equal amplitude and 90° phase difference. Due to the broadband and stable 90° phase difference of the balun, the polarization purity and 3-dB axial ratio bandwidth of the proposed antenna are improved. The measured results show that impedance bandwidth of 70.2%, ARBW of 61%, port isolation of 15 dB, and dual sense circular polarization are obtained with the proposed design, which could be a good candidate for the application in WiMAX and WLAN.

ACKNOWLEDGMENT

This work is supported by the National Key Research and Development Project No. 2017YFC0804404 and Key Projects of Natural Science Research in Higher Education Institutions of Anhui Province, Grant Number: No. KJ2016A663.

REFERENCES

1. Sze, J. Y. and C. C. Chang, "Circularly polarized square slot antenna with a pair of inverted-L ground strips," *IEEE Antennas Wireless Propag. Lett.*, Vol. 7, 149–151, 2008.
2. Yang, W. W., J. Y. Zhou, Z. Q. Yu, and L. S. Li, "Single-fed low profile broadband circularly polarized stacked patch antenna," *IEEE Trans. Antennas Propag.*, Vol. 62, No. 10, 5406–5410, Oct. 2014.
3. Ding, K., C. Gao, D. Qu, and Q. Yin, "Compact broadband circularly polarized antenna with parasitic patches," *IEEE Trans. Antennas Propag.*, Vol. 65, No. 9, 4854–4857, Sep. 2017.
4. Baik, J. W., T. H. Lee, and S. Pyo, "Broadband circularly polarized crossed dipole with parasitic loop resonators and its arrays," *IEEE Trans. Antennas Propag.*, Vol. 59, No. 1, 80–88, Jan. 2011.
5. Ta, S. X. and I. Park, "Compact wideband circularly polarized patch antenna array using metasurface," *IEEE Antennas Wireless Propag. Lett.*, Vol. 16, 1932–1936, 2017.
6. Narbudowicz, A., X. L. Bao, and M. J. Ammann, "Dual circularly-polarized patch antenna using even and odd feed-line modes," *IEEE Trans. Antennas Propag.*, Vol. 61, No. 9, 4828–4831, Sep. 2013.
7. Khan, M., Z. C. Yang, and K. Warnick, "Dual-circular-polarized high-efficiency antenna for Ku-band satellite communication," *IEEE Antennas Wireless Propag. Lett.*, Vol. 13, 1624–1627, 2014.
8. Kumar, K., S. Dwari, and M. K. Mandal, "Broadband dual circularly polarized substrate integrated waveguide antenna," *IEEE Antennas Wireless Propag. Lett.*, Vol. 16, 2971–2974, 2017.
9. Jin, C., R. Li, A. Alphones, and X. Bao, "Quarter-mode substrate integrated waveguide and its application to antenna design," *IEEE Trans. Antennas Propag.*, Vol. 61, No. 6, 2921–2928, Jun. 2013.
10. Cai, Y., Y. Zhang, Z. Qian, W. Cao, and S. Shi, "Compact wideband dual circularly polarized substrate integrated waveguide horn antenna," *IEEE Trans. Antennas Propag.*, Vol. 64, No. 7, 3184–3188, Feb. 2016.